JOURNAL OF CATALYSIS **173,** 122–133 (1998)
ARTICLE NO. CA971923

LHHW and PSSA Kinetic Analysis of Rates and Adsorbate Coverages in $CO/H_2/C_2H_4$ Reactions on $Mn–Rh/SiO_2$

Mark A. Brundage,[1] Michael W. Balakos,[2] and Steven S. C. Chuang[3]

Department of Chemical Engineering, The University of Akron, Akron, Ohio 44325-3906

Received March 11, 1997; revised October 1, 1997; accepted October 3, 1997

The kinetics, adsorbate residence times and coverages, and isotopic transient responses for propionaldehyde formation from $CO/H_2/C_2H_4$ reaction have been studied over 4 wt% $Mn–Rh/SiO_2$ ($Mn:Rh = 0.1:1$) catalyst at 513 K and 0.1 MPa. Reaction rates were measured under differential conditions; adsorbate residence times and coverages, and transient responses of ^{13}C propionaldehyde formation were measured by a steady-state isotopic transient method coupled with *in situ* infrared spectroscopy. Both Langmuir–Hinselwood–Hougen–Watson (LHHW) and pseudo-steady-state-approximation (PSSA) approaches were employed to develop rate laws (i.e., kinetic models) and isotherm equations for adsorbate coverages to fit the rate and coverage data. Although the LHHW kinetic model provides a good fit of the rate data, its adsorbed acyl ($^*C_2H_5CO$) isotherm equation fails to describe the dependence of adsorbed acyl coverage on H_2 and CO partial pressures. Use of the PSSA approach without assumption of a sole rate-determining step (RDS) resulted in a rate law and an acyl isotherm equation which describe both the kinetics and adsorbate coverages behaviors with high accuracy. The PSSA analysis suggests that both CO insertion into adsorbed ethyl species and hydrogenation of adsorbed acyl species are kinetically significant steps for propionaldehyde formation. The failure of LHHW isotherm equations for fitting the coverage data is due to lack of a sole RDS. The kinetics, adsorbate residence times and coverages, and transient responses of propionaldehyde formation on $Mn–Rh/SiO_2$ were compared with those on Rh/SiO_2 to unravel the effect of Mn promotion on the reaction. This study demonstrates that measurement of transient responses for product formation and adsorbate residence times and coverages provides essential information for verification of kinetic models with mechanistic significance.

INTRODUCTION

Promoters play a significant role in modifying the activity and selectivity of CO hydrogenation on supported Rh catalysts. Different additives have a specific effect on the activity and selectivity of the overall reaction (1–3): alkali promoters increase the selectivity of oxygenate synthesis (4–6); S and Ag additives have been shown to increase the selectivity of higher oxygenates by decreasing the rate of hydrogenation (7, 8); ZnO, CaO, and MgO enhance the production of methanol (9); oxides such as Mn, Zr, and Ti increase the overall rate of CO conversion (10–12). Among these additives, Mn has shown a dramatic promotion effect which increases the overall rate of CO conversion by at least an order of magnitude but does not significantly change the selectivity in CO hydrogenation (12).

The specific contribution of Mn in these specific surface reactions has been the subject of many studies (10, 13–18). The addition of Mn to Rh/SiO_2 does not significantly change the dispersion of the Rh metal on the support (10, 17). Electron spin resonance (ESR) spectroscopy revealed that Mn is not readily reduced and is of the MnO form after exposure to H_2 at 773 K (19). Infrared (IR) spectroscopy studies on promoted catalysts show that carbon monoxide is adsorbed as linear and bridged CO, much like that of an unpromoted catalyst, and a broad band in the 1650–1775 cm^{-1} region that is assigned to a tilted CO species according to the cluster–surface analogy (10, 16, 18). It is proposed that the low wavenumber of the tilted CO is a result of the interaction of the oxygen end of the adsorbed CO with the oxophilic Mn additive. The proposed interaction resembles the interaction of a Lewis acid with a CO ligand of a metal carbonyl, causing a downward shift of the CO ligand wavenumber to below 1700 cm^{-1} (20, 21). This type of adsorbed CO has been suggested to be a precursor to CO dissociation and CO insertion. Thus, the presence of such a species increases the rate of both surface reactions (10). Although this low wavenumber species has been observed on Mn promoted catalysts, there is no evidence of the participation of this species in the surface CO insertion reaction (13, 22).

Heterogeneous hydroformylation has been used as an effective probe reaction for studying the hydrogenation and CO insertion activities of transition metal catalysts without complication of the CO dissociation step (4, 5, 7, 10, 23, 24). In ethylene hydroformylation, ethylene is partially hydrogenated to form an adsorbed ethyl species. Hydrogenation of adsorbed ethyl leads to ethane; the insertion of linear

[1] Present address: Delphi, Rochester, NY.
[2] Present address: United Catalysts Inc., Louisville, KY.
[3] To whom correspondence should be addressed.

0021-9517/98 $25.00

CO into adsorbed ethyl species (or ethyl migration onto adsorbed CO) results in the formation of a postulated adsorbed acyl species which can be further hydrogenated to form propionaldehyde (4, 5, 7, 10). The selectivity toward ethane and propionaldehyde reflects the relative activity of the catalyst for hydrogenation and CO insertion. Investigation of the selectivity of Mn-promoted Rh catalyst from ethylene hydroformylation may reveal the role of Mn in CO insertion and hydrogenation.

The objectives of this study are to utilize *in situ* IR spectroscopy combined with steady-state isotopic transient method to determine how Mn modifies the overall rate law for ethane and propionaldehyde formation, the surface coverage of reaction intermediates, and the reactivity and residence times of adsorbates during heterogeneous hydroformylation on a $Mn{-}Rh/SiO_2$ catalyst. The coverage of adsorbed CO was measured by IR spectroscopy; the residence time, the distribution of rate constants, and the coverage of intermediates leading to the formation of propionaldehyde were measured by steady-state isotopic transient method (24–26). Both Langmuir–Hinshelwood–Hougen–Watson (LHHW) and pseudo-steady-state-approximation (PSSA) approaches were used to derive the rate law (i.e., kinetic models) for propionaldehyde and ethane formation and isotherm equations for coverage of adsorbed CO and C_2H_5CO intermediates from various proposed mechanisms and postulations. The kinetic models and isotherm equations for coverage were tested by comparing the model rates and coverage with the measured rates of product formation and adsorbate coverage. Testing of the kinetic model by analysis of the macroscopic rate data and coverage data reduces the uncertainty in identifying the rate-determining step (RDS), and thus the rational reaction mechanism. The results of the $Mn{-}Rh/SiO_2$ catalyst were compared to the unpromoted Rh/SiO_2 to determine the role of Mn as a promoter in CO insertion and the validity of LHHW and PSSA kinetic analysis approach for heterogeneously catalyzed reactions.

EXPERIMENTAL

Catalyst Preparation and Characterization

A 4 wt% Rh/SiO_2 catalyst was made by impregnating an aqueous solution of $RhCl_3 \cdot 3H_2O$ (Alfa Products) into large pore SiO_2 support (Strem Chemicals, surface area of 350 m^2/g). The ratio of the volume of solution to the weight of silica support used in the impregnation step was 1 cm^3 to 1 g. After impregnation, the sample powder was dried in air at 298 K overnight and then reduced in flowing hydrogen at 673 K for 16 h. The $Mn{-}Rh/SiO_2$ catalyst was prepared by sequential impregnation of the unpromoted catalyst with an aqueous solution of $Mn(NO_3)_2 \cdot 6H_2O$ ($Mn/Rh = 0.1$). The sample was dried at 298 K overnight and further reduced at 673 K for 16 h. Catalyst that was made by co-impregnation of Mn and Rh at $Mn:Rh = 0.5$ and 1 onto a silica support did not exhibit a band in the tilted CO region during CO chemisorption study. The hydrogen uptake was determined to be 122 $\mu mol/g_{cat}$ for Rh/SiO_2 and 114 $\mu mol/g_{cat}$ for $Mn{-}Rh/SiO_2$ corresponding to Rh particle sizes of 15 and 16 Å, respectively, by H_2 pulse chemisorption method at 303 K. These results are consistent with previous results in the literature where the addition of Mn did not significantly influence the amount of H_2 chemisorption at room temperature (10, 17).

Experimental Apparatus and Procedure

The apparatus used in this study is similar to that previously reported (27) and will be briefly discussed here. Approximately 60 mg of catalyst powder was pressed into three self-supporting disks. One disk was placed directly in the pathway of the IR beam in the reactor cell and the other two disks were broken up and placed in the outlet stream of the reactor producing enough products for accurate determination of the product transient response by mass spectrometer. The IR reactor cell, which can be operated up to 773 K and 1 MPa, acts as a differential reactor, allowing measurement of the initial rates for the forward reaction. Prior to the experiments, the catalyst was further reduced under H_2 flow at 673 K and 0.1 MPa for 2 h. The reactant gases of $CO/H_2/C_2H_4/He$ were passed over the catalyst at a desired ratio and a total flow rate of 120 cm^3/min. Helium was used as a diluent and for maintaining a constant total flow rate of 120 cm^3/min, while varying the partial pressure of an individual reactant. The reactant flow rates were controlled by mass flow controllers and were combined at a mixing point before entering the IR reactor cell.

After the reaction attained steady state (about 5–10 min as determined by on-line mass spectrometry), the steady-state concentrations of the gaseous products were also analyzed by an HP-5890A gas chromatograph equipped with a FID detector. Following the steady-state measurement, a Valco 6-port valve was utilized to introduce a 10 cm^3 pulse of ^{13}CO into the CO stream, while maintaining the steady-state flows of H_2 and C_2H_4. The pressure within the sampling loop of the 6-port pulsing valve was equal to that of the reactor influent so that the steady-state flow was maintained during the pulse injection of ^{13}CO. The ^{12}CO stream contained 2% Ar for determining the effect of gas-phase holdup in the reactor and the gas transportation lines on the transient response of gaseous products. Subtracting the residence time of Ar from that of the product species reveals the residence time of the adsorbed intermediates leading to the specific product.

The transient response of adsorbed CO was recorded by the IR spectrometer. The *in situ* IR spectra were recorded

by a Nicolet 5SXC spectrometer with a DTGS detector at a resolution of 4 cm^{-1}. Thirty-two scans were coadded when recording spectra under steady-state conditions while only three scans were coadded under transient conditions to facilitate rapid scanning. The transient responses of the gaseous reactants and products from the IR cell were recorded by a Balzers QMG112 mass spectrometer (MS) interfaced to a microcomputer. The MS is equipped with a differentially pumped inlet system located directly downstream of a pressure regulator for rapid response to the change in gaseous composition in the reactor effluent. The *m/e* ratios monitored by the MS were 28 for CO, 29 for ^{13}CO, 40 for Ar, and 59 for $C_2H_5{}^{13}CHO$. The *m/e* ratios were carefully selected to prevent interference from the fragmentation of parent species.

After each transient experiment, a bracketing technique (28) was used whereby the catalyst was heated under a H_2 atmosphere to 573 K in 10 min, held at 573 K for 10 min, and then cooled to the reaction temperature for 10 min to start the next experiment. This technique prevented deactivation and yielded good reproducibility as evidenced by a relative standard deviation (standard deviation/mean × 100) of 2.5 between experimental runs.

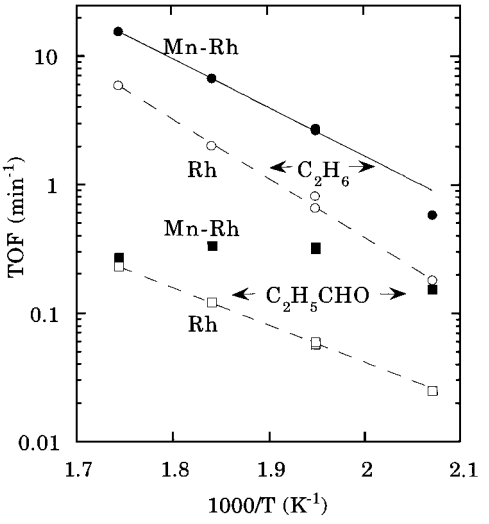

FIG. 1. Arrhenius plot of ethane and propionaldehyde formation on Rh/SiO_2 and $Mn{-}Rh/SiO_2$ at 0.1 MPa and $CO/H_2/C_2H_4/He = 1/1/1/1$. Solid symbols represent Mn–Rh and open symbols represent Rh. Lines are plotted from Arrhenius equation.

RESULTS

Steady-State Measurements

Table 1 lists the turnover frequencies (TOF) of all the hydrocarbon and oxygenated products in the temperature range 483–573 K and a $CO/H_2/C_2H_4/He$ ratio of 1/1/1/1 under steady-state flow conditions. TOF is defined as the rate of product formation divided by the amount of surface exposed Rh metal atoms as measured by H_2 chemisorption. The main products of the reaction at 483 and 513 K are propionaldehyde, the product of CO insertion, and ethane, the product of ethylene hydrogenation. The products other than propionaldehyde and ethane constitute 5.9% of all the products at 483 K. This amount increased to about 14% at 513 K and decreased again to 5.7% at 573 K. The propionaldehyde selectivity decreased with increasing temperature.

Figure 1 shows the Arrhenius plot of ethane and propionaldehyde formation rates on the Rh/SiO_2 and $Mn{-}Rh/SiO_2$ catalyst. The Rh/SiO_2 results have been previously reported (29) and are shown as dashed lines in the figures for comparison. The dependence of ethane formation rate on temperature follows the Arrhenius law with an activation energy of 19.6 kcal/mol, while the propionaldehyde formation rates reach a maximum 543 K and decreases slightly at 573 K, digressing from linearity in the Arrhenius plot. The deviation from linearity in propionaldehyde formation has also been observed on S-, Ag-, and Cu-promoted Rh/SiO_2 catalysts and is attributed to the

TABLE 1

Reaction Rate and Selectivity in Heterogeneous Hydroformylation on $Mn{-}Rh/SiO_2$[a] for $CO/H_2/C_2H_4/He = 1/1/1/1$ and a Total Flowrate of 120 cm^3/min

Temperature (K)	Turnover frequency of product formation ($10^3 \cdot min^{-1}$)[b]								Selectivity[c]
	CH_4	C_2H_6	C_2H_5CHO	C_3H_6	C_4H_8	n-C_4H_{10}	C_5H_{10}	C_5H_{12}	
483	32.8	578	154	10.2	—	2.09	0.746	—	0.267
513	105	2750	314	178	54.9	108	22.5	8.82	0.114
513	121	2655	324	187	62.1	121	20.3	12.0	0.122
543	195	6700	333	316	99.9	213	34.1	15.6	0.050
573	253	15500	269	387	110	200	—	—	0.017

[a] Silica purity: 99.5% SiO_2, 0.02% Fe, 0.09% Na_2O.
[b] The TOF reported in this table are multiplied by 10^3.
[c] Selectivity is defined as $TOF_{C_2H_5CHO}/TOF_{C_2H_6}$.

dominance of hydrogenation over CO insertion at temperatures above 543 K (30).

To determine the dependence of the reaction rates on the partial pressure of the reactants, the TOFs (rates) of ethane and propionaldehyde formation were measured as the function of partial pressures of the reactants at a total pressure of 0.1 MPa and 513 K. Figure 2 shows the log–log plots of the TOF for ethane and propionaldehyde formation versus P_{CO}, P_{H_2}, and $P_{C_2H_4}$ (i.e., the partial pressures of CO, H_2, and C_2H_4). Both ethane and propionaldehyde formation rates show positive order in P_{H_2} and $P_{C_2H_4}$. Ethane rate formation is negative order in P_{CO}, indicating that the adsorption of CO suppresses ethylene hydrogenation. Propionaldehyde formation rate exhibits positive order in P_{CO} on Mn–Rh/SiO_2, but negative order in P_{CO} on Rh/SiO_2.

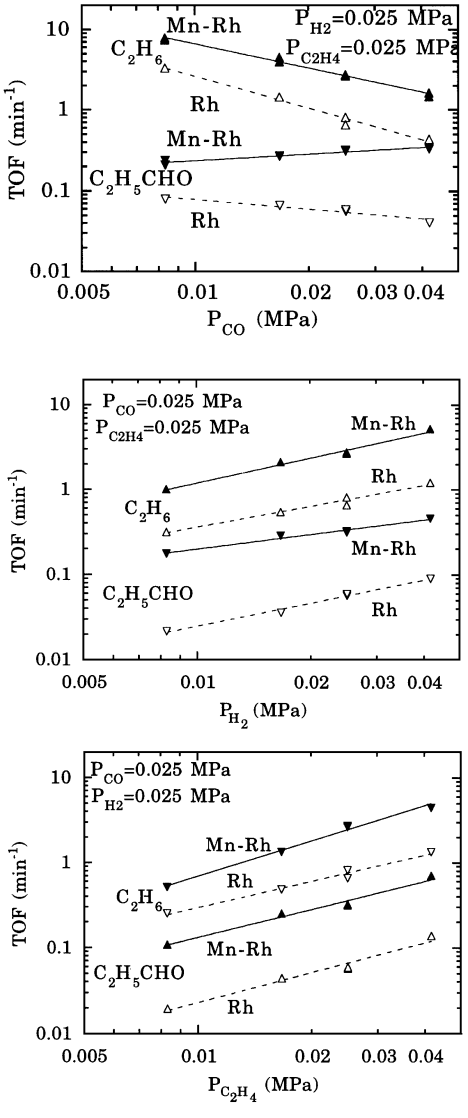

FIG. 2. Dependence of rate of ethane and propionaldehyde formation on the reactant partial pressures at 513 K and a total pressure of 0.1 MPa. He served as a diluent to make the total pressure 0.1 MPa. Solid symbols represent Mn–Rh and open symbols represent Rh. Lines are plotted from power law equations in Table 3.

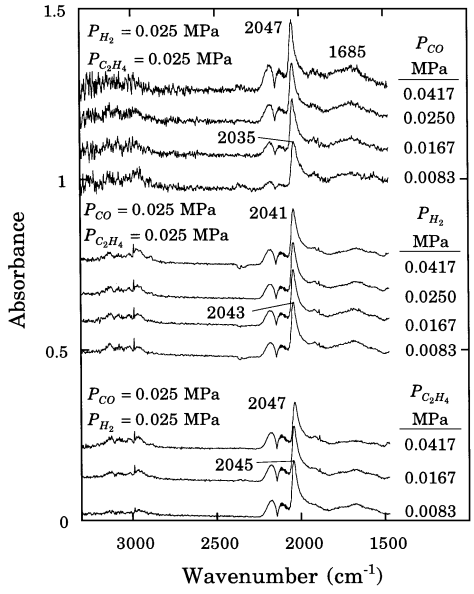

FIG. 3. *In situ* IR spectra of heterogeneous hydroformylation on Mn–Rh/SiO_2 at 0.1 MPa and 513 K at varying reactant partial pressures.

The infrared spectra taken during the steady-state runs are shown in Fig. 3. The series at different P_{CO} contain a lower signal-to-noise ratio because these experiments were taken at a faster mirror speed in the FTIR spectrometer. The presence of gas phase CO is indicated by the bands at 2120 and 2180 cm^{-1}. This series also shows that the wavenumber number of the linear CO band at 2035 cm^{-1} increases to 2047 cm^{-1} as P_{CO} is increased. The increase in the band wavenumber is due to an increase in dipole–dipole interaction resulting from increasing surface coverage of CO (31). Figure 3 also shows the appearance of a broad band at 1685 cm^{-1}. This band is attributed to the titled mode of adsorbed CO in which the carbon end is coordinated to the reduced Rh metal and the oxygen end is coordinated to the Mn promoter (13, 16). The titled CO band intensity slightly increased with increasing P_{CO}, did not significantly change with P_{H_2}, and decreased slightly with increasing $P_{C_2H_4}$. Changes in the IR spectra of the gaseous hydrocarbon region (~3000 cm^{-1}) were not able to be distinguished.

Dynamic Measurements

The transient response of $C_2H_5{}^{13}CHO$ and the IR spectra to a 10 cm^3 pulse of ^{13}CO into the CO feed to the IR reactor cell were recorded during the steady-state isotopic transient experimental runs. Figure 4 shows the transient responses of Ar, ^{13}CO, and $C_2H_5{}^{13}CHO$ measured by mass spectrometry under the conditions of 0.1 MPa, 513 K, and $CO/H_2/C_2H_4/He = 1/1/1/1$. For convenience the Ar

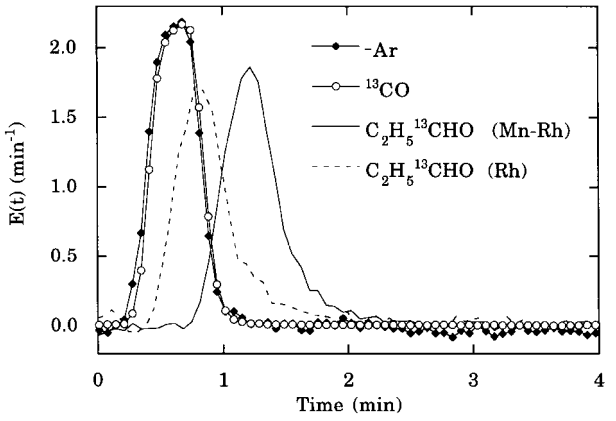

FIG. 4. The transient responses of Ar, ^{13}CO, and $C_2H_5{}^{13}CHO$ to a pulse of ^{13}CO in the ^{12}CO feed during ethylene hydroformylation on Mn–Rh/SiO_2 at 513 K and 0.1 MPa. (The dashed line represents the $C_2H_5{}^{13}CHO$ response on Rh/SiO_2; Ar and ^{13}CO are equivalent for both Rh/SiO_2 and Mn–Rh/SiO_2. ^{12}CO which exhibited a negative response is not included in Fig.)

response is shown in Fig. 4 as the mirror image of the actual response. For comparison, the responses are normalized to $E(t)$,

$$E(t) = \frac{C(t)}{\int_0^\infty C(t)dt}, \qquad [1]$$

where $C(t)$ is the concentration during the transient. The time delay in the ^{13}C propionaldehyde response as compared to the ^{13}CO response is equivalent to the residence time of ^{13}C surface intermediates leading to ^{13}C propionaldehyde which is derived from ^{13}CO. An interesting feature of the propionaldehyde response on the Mn–Rh/SiO_2 catalyst as compared to the Rh/SiO_2 response is the 0.5 min delay prior to the initial ^{13}C propionaldehyde response. This delay cannot be attributed mainly to the readsorption effect and will be discussed later.

Figure 5a shows the IR spectra recorded during the isotopic pulse corresponding to the MS response shown in Fig. 4. Figure 5a shows that gaseous ^{12}CO is replaced by ^{13}CO in the reactor for approximately 0.7 min, then returns to the original ^{12}CO flow. The dashed lines in Fig. 5a highlight the decrease in gas phase ^{12}CO and the appearance of gas phase ^{13}CO IR intensities. Not all the gas phase ^{12}CO is flushed from the IR reactor by the ^{13}CO pulse. This is due to the fact that the pulse volume is not large enough to totally remove the flowing ^{12}CO. The intensity of the linear ^{13}CO grew as high as that of linear ^{12}CO at 0.4 min, indicating that the majority of the linear ^{12}CO was replaced by ^{13}CO. The exchange of the adsorbed linear ^{12}CO at 2045 cm^{-1} with linear ^{13}CO at 1993 cm^{-1} occurred at a rate as rapid as the gaseous $^{12}CO/^{13}CO$ exchange.

Figure 5b shows the difference spectra (i.e., the spectra recorded at time t subtracted from the spectra at $t=0$), which better represent the changes in adsorbates on the surface during the pulse. The exchange between gaseous ^{12}CO and ^{13}CO in Fig. 4 corresponds to the exchange between linear ^{12}CO and ^{13}CO in the IR spectra of Fig. 5b, indicating that the gas phase CO and adsorbed CO exchange with their isotopic counterparts at a rate much faster than

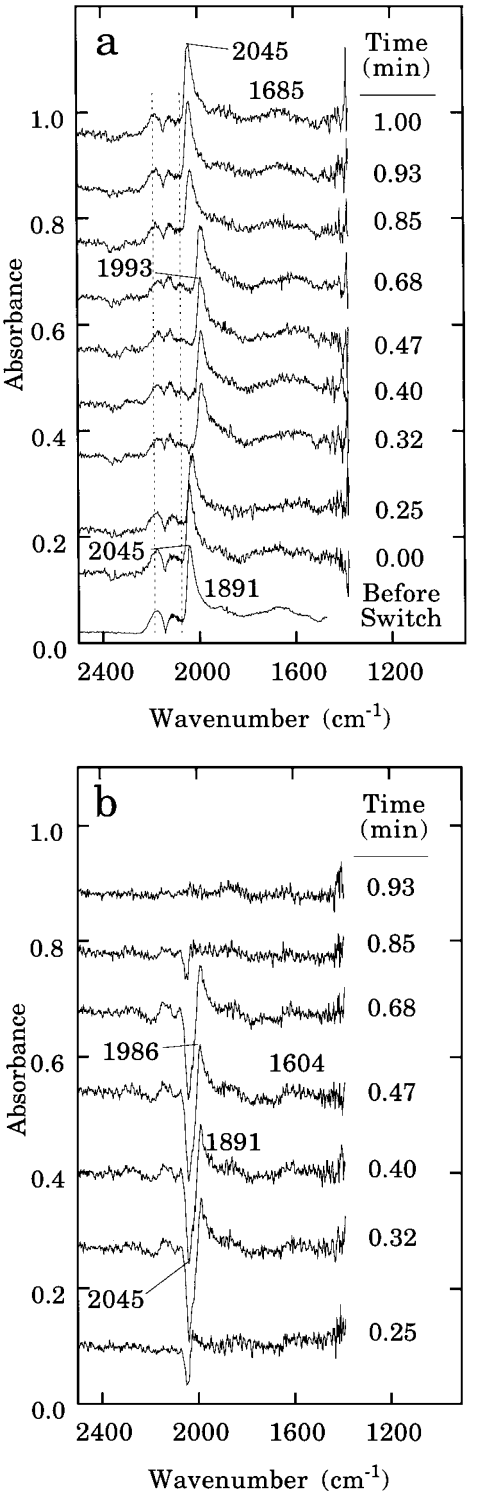

FIG. 5. (a) The *in situ* IR response to a pulse of ^{13}CO in the ^{12}CO feed. (b) The difference spectra during a pulse of ^{13}CO in the ^{12}CO feed.

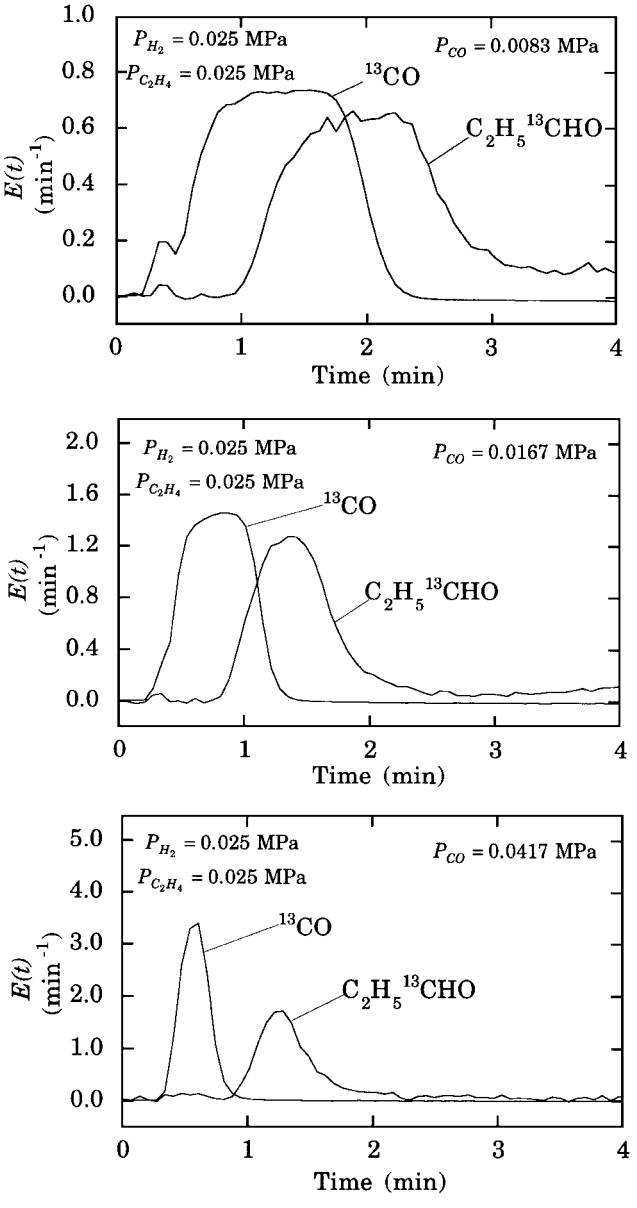

FIG. 6. The transient responses of ^{13}CO and $C_2H_5{}^{13}$CHO to a pulse of ^{13}CO in the ^{12}CO feed during ethylene hydroformylation for varying P_{CO} on Mn–Rh/SiO_2.

the scanning rate of the IR. A broad band in the difference spectra may be discerned in the 1604 cm^{-1} region. This band is assigned to the tilted form of adsorbed ^{13}CO. No other feature in the IR spectra changed during the experiment, including those attributed to gaseous ethylene. The same conclusions can be drawn for all the spectra recorded during all the transient experiments.

Figure 6 shows the transient responses of ^{13}CO and $C_2H_5{}^{13}$CHO during a pulse of ^{13}CO into the ^{12}CO feed for P_{CO} of 0.0083, 0.0167, and 0.0417 MPa at constant partial pressures of P_{H_2} and $P_{C_2H_4}$ at 0.025 MPa each. Variation of CO partial pressure is achieved by altering the CO flow rate with helium as a diluent to obtain a constant total flow rate at 120 cm^3/min. Since 10 cm^3 of ^{13}CO is pulsed into the steady-state ^{12}CO flow, the variation in ^{12}CO flow rate caused variation in the residence time of ^{13}CO. The decrease in the residence time of ^{13}CO with increasing P_{CO} in each figure is due to increasing the CO flow rate (i.e., increasing P_{CO}) which more quickly flushes the 10 cm^3 of ^{13}CO to the reactor from the pulsing loop. Figure 6 shows that increasing P_{CO} causes a clearer separation between $C_2H_5{}^{13}$CHO and ^{13}CO responses, suggesting that increasing P_{CO} may vary the residence time of intermediates leading to propionaldehyde. Increasing P_{CO} has also been shown to increase the TOF for propionaldehyde formation as shown in Fig. 2.

Figure 7 shows how the responses of ^{13}CO and $C_2H_5{}^{13}$CHO vary with respect to changes in P_{H_2} and $P_{C_2H_4}$. The

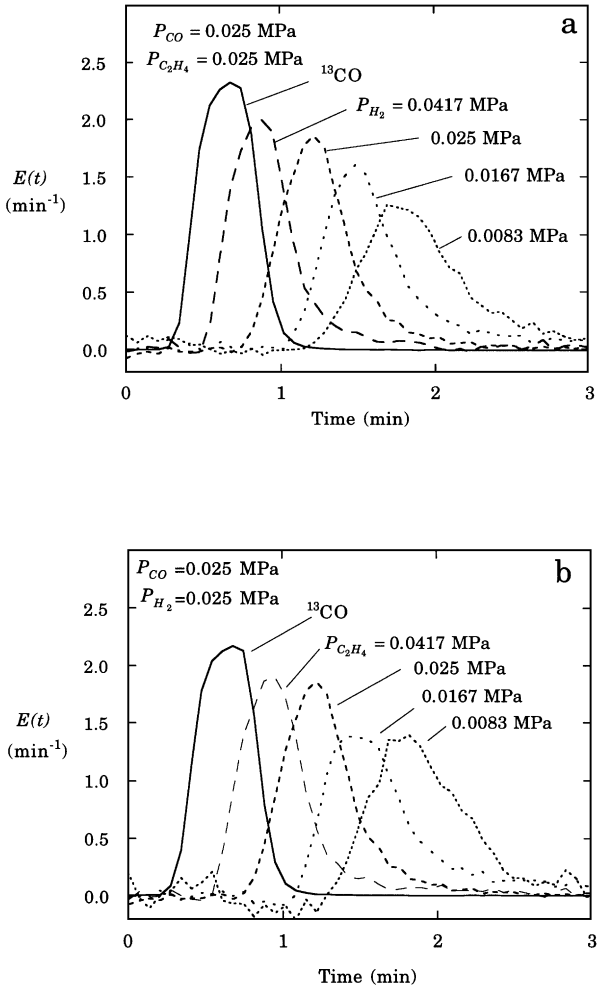

FIG. 7. (a) The transient responses of ^{13}CO and $C_2H_5{}^{13}$CHO to a pulse of ^{13}CO in the ^{12}CO feed during ethylene hydroformylation for varying P_{H_2}. (b) The transient response of ^{13}CO and $C_2H_5{}^{13}$CHO to a pulse of ^{13}CO in the ^{12}CO feed during ethylene hydroformylation for varying $P_{C_2H_4}$ on Mn–Rh/SiO_2.

response of ^{13}CO did not vary in these experiments because the CO flow rate was kept constant. Figure 7 shows that as P_{H_2} and $P_{C_2H_4}$ increased, the residence time of intermediates leading to the formation of propionaldehyde decreased. Following the derivation of the transient equations in a previous study (29), the average residence time of all intermediate species leading to the formation of ^{13}C propionaldehyde from adsorbed ^{13}CO can then be expressed as

$$\tau_{C_2H_5{}^{13}CHO} = \int_0^\infty t E_{C_2H_5{}^{13}CO}(t)dt - \tau_{^{13}CO}, \qquad [2]$$

where τ is the residence time, $E(t)$ is defined in Eq. [1], and t is the time. Figure 8 shows the variation of $\tau_{C_2H_5{}^{13}CHO}$ with the reactant partial pressure. Increasing P_{CO} caused a slight decrease in the average residence time of $C_2H_5{}^{13}CHO$ on Mn–Rh/SiO_2, while increasing P_{H_2} and $P_{C_2H_4}$ caused a marked decrease in the average residence time of $C_2H_5{}^{13}CHO$. Since the total flow rate for all of the pulse transients was kept constant, the variation of the transient response and delay time with reactant partial pressure suggests the long delay time prior to the initial $C_2H_5{}^{13}CHO$ response cannot be attributed to readsorption effect. Increasing the total flow rate of reactants from 120 to 240 cm^3/min did not cause a significant variation in $\tau_{C_2H_5{}^{13}CHO}$, further confirming that readsorption does not play a significant role in causing the delay in $C_2H_5{}^{13}CHO$ response.

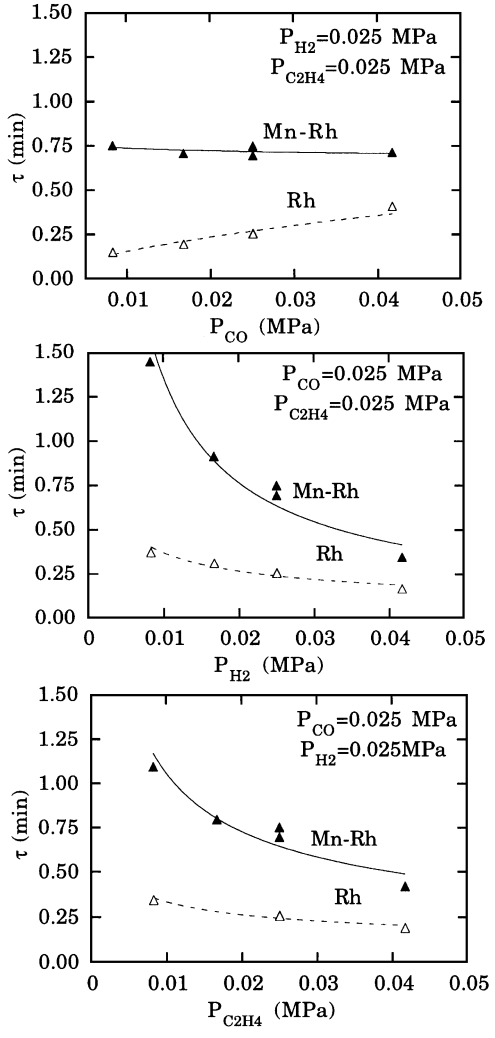

FIG. 8. Variation of $\tau_{C_2H_5CHO}$ as a function of the reactant partial pressures. Solid symbols represent Mn–Rh and open symbols represent Rh. Lines are included to display trend.

An estimate of the surface coverage of all intermediate species leading to the formation of propionaldehyde can be calculated by

$$\theta_{*C_2H_5CO} = \tau_{C_2H_5{}^{13}CHO} \cdot \mathrm{TOF}_{C_2H_5CHO}. \qquad [3]$$

The acyl surface coverage, $\theta_{*C_2H_5CO}$, is defined as the summation of coverages of all intermediates in the reaction between *CO and the propionaldehyde product. In the LHHW II model, it was assumed that the $^*C_2H_5CO$ (acyl) hydrogenation is the rate-determining step for propionaldehyde formation. This assumption suggests $^*C_2H_5CHO$ species desorbs as soon as it is formed to form gaseous propionaldehyde. As a result, $\theta_{*C_2H_5CO} \gg \theta_{*C_2H_5CHO}$ and the surface coverage measured by the transient isotopic method is approximately equal to the surface coverage of the acyl intermediate, $\theta_{*C_2H_5CO}$. Lumping $\theta_{*C_2H_5CO}$ and $\theta_{*C_2H_5CHO}$ into one pool as $\theta_{*C_2H_5CO}$ can be further justified by an approximated first-order response for all the $C_2H_5{}^{13}CHO$ responses to a ^{13}CO pulse input in Figs. 6 and 7 (24). Equations [2] and [3] were used to obtain $\theta_{*C_2H_5CO}$, shown in Fig. 9, from the transient responses of the ^{13}C labeled gaseous CO and propionaldehyde at various reactant partial pressures. The results show that $\theta_{*C_2H_5CO}$ increases with increasing P_{CO} and $P_{C_2H_4}$, but decreases with increasing P_{H_2}.

DISCUSSION

Reaction Mechanism

The proposed mechanism for heterogeneous hydroformylation is presented in Table 2 (24, 29). The formation of propionaldehyde involves the partial hydrogenation of C_2H_4 to form an adsorbed ethyl ($^*C_2H_5$) species, insertion of adsorbed linear CO into the adsorbed ethyl species to form an adsorbed acyl species ($^*C_2H_5CO$), and hydrogenation of the acyl species to produce propionaldehyde. Hydrogenation of the adsorbed ethyl species results in the formation of ethane. The same type of surface-adsorbed hydrogen and ethyl species is assumed to participate in the formation of both ethane and propionaldehyde. The rates of formation for other minor products are not considered in the present study.

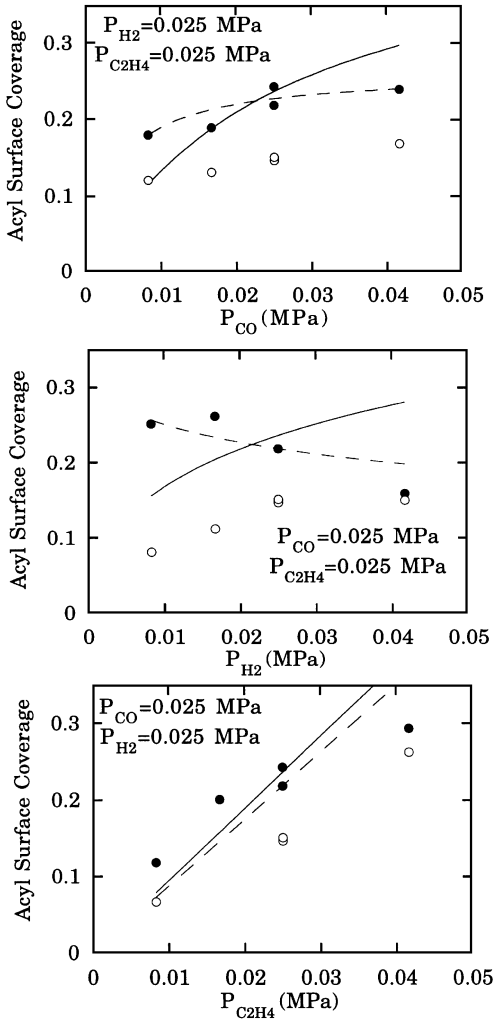

FIG. 9. Adsorption isotherms of reaction intermediates as a function of partial pressures of reactants. Solid symbols represent Mn−Rh and open symbols represent Rh X10. Solid lines are plotted from Eq. [6]. Dashed lines are plotted from Eq. [13].

Kinetic Modeling

The rate law (rate equation or expression) for heterogeneously catalyzed reactions may be expressed in the form of a power law, Langmuir–Hinshelwood–Hougen–Watson, and Temkin kinetics (29, 32). Temkin kinetics has been used especially for description of kinetics of ammonia synthesis on nonuniform surfaces (33, 34). The power law expression provides limited insight into the reaction mechanism and may be considered as a limiting case of the LHHW kinetics. The power law listed in Table 3 can be obtained by fitting the rate data to

$$\hat{\mathrm{TOF}} = k \prod_{i=1}^{I} P_i^{\alpha_i}, \qquad [4]$$

where $\hat{\mathrm{TOF}}$ is the estimated kinetic model TOF, k is the rate constant, i represents the individual reactants, α_i is the reaction order of each individual reactant, and $\prod_i^I$ is the symbol for the product of P_i terms,. All the TOFs versus reactant partial pressure data in Fig. 2 were fit simultaneously to determine the reactant order by a nonlinear least squared approximation for both propionaldehyde and ethane using Microsoft Excel spreadsheet. The solid lines in Fig. 2 are from the power law equations in Table 3.

Although rate data of many heterogeneously catalyzed reactions have been shown to fit well to LHHW kinetic models (35, 36), the mechanism identified by the goodness of data fitting to the model has been the subject of much criticism due to questionable assumptions of uniform active sites and absence of adsorbate–adsorbate interactions as well as the number of adjustable parameters, typically more than three, in the model equation (29, 32–34, 36). Most of the criticisms are a result of the inability to measure the rate constant (reactivity of sites) distribution, adsorbate–adsorbate interactions, the adsorbate coverages, and reaction intermediates as a function of partial pressure of reactants as well as the inability to identify the RDS.

Our recent isotopic transient studies measured the rate constant distribution as well as adsorbate residence times and coverages for $CO/H_2/C_2H_4$ reaction on Rh/SiO_2 revealing that propionaldehyde formation takes place on the site exhibiting a single, sharp distribution; LHHW kinetic model and its adsorbate isotherm equation describe rate and coverage data with high accuracy (29). The ability of LHHW kinetics to model the data and to describe the reaction and its RDS has been attributed to the structure insensitivity of the reaction (29, 34), the single sharp distribution of sites, and the dominance of CO adsorbates diminishing other adsorbate–adsorbate interactions (29). These attributes have also been observed for the reaction on $Mn{-}Rh/SiO_2$. Steps involved in the formation of propionaldehyde such as hydrogenation are known to be structure-insensitive; CO insertion which has been shown to occur on single Rh sites is also structure-insensitive. Rate constant analysis shows that reactivity distribution of sites for propionaldehyde formation on $Mn{-}Rh/SiO_2$ is as sharp as that for Rh/SiO_2, indicating that the active sites for propionaldehyde formation on $Mn{-}Rh/SiO_2$ are as uniform as those on Rh/SiO_2. Uniformity of the propionaldehyde formation site is further evidenced by the parallel ^{13}CO and $C_2H_5{}^{13}CHO$ responses shown in Figs. 4 and 6. The lack of significant interaction between adsorbed CO is reflected in the absence of marked variation of wavenumber of adsorbed CO with partial pressure of H_2 and C_2H_4 as shown in Fig. 3. Thus, dynamic and LHHW approaches employed in the analysis of data for Rh/SiO_2 (29) may be applied for analysis of $Mn{-}Rh/SiO_2$ data.

The development of LHHW kinetic models requires the assumption of a rate-determining step for each product. By comparing the proposed mechanism for both

TABLE 2

Proposed Mechanism for Heterogeneous Hydroformylation

	Reaction steps	Surface coverage[a]
Step 1	$H_2(g) + 2^{*\,b} \overset{K_1{}^c}{} 2^*H$	$\theta_{*H} = \frac{(K_1 P_{H_2})^{1/2}}{1+(K_1 P_{H_2})^{1/2}+K_2 P_{CO}+K_3 P_{C_2H_4}}$
Step 2	$CO(g) + * \overset{K_2}{} {}^*CO$	$\theta_{*CO} = \frac{K_2 P_{CO}}{1+(K_1 P_{H_2})^{1/2}+K_2 P_{CO}+K_3 P_{C_2H_4}}$
Step 3	$C_2H_4(g) + * \overset{K_3}{} {}^*C_2H_4$	$\theta_{*C_2H_4} = \frac{K_3 P_{C_2H_4}}{1+(K_1 P_{H_2})^{1/2}+K_2 P_{CO}+K_3 P_{C_2H_4}}$
Step 4	$^*C_2H_4 + {}^*H \overset{K_4}{} {}^*C_2H_5 + *$	$\theta_{*C_2H_5} = \frac{(K_1 P_{H_2})^{1/2} K_3 K_4 P_{C_2H_4}}{1+(K_1 P_{H_2})^{1/2}+K_2 P_{CO}+K_3 P_{C_2H_4}}$
Step 5	$^*C_2H_5 + {}^*CO \overset{K_5}{} {}^*C_2H_5CO + *$	$\theta_{*C_2H_5CO} = \frac{(K_1 P_{H_2})^{1/2} K_2 K_3 K_4 K_5 P_{CO} P_{C_2H_4}}{1+(K_1 P_{H_2})^{1/2}+K_2 P_{CO}+K_3 P_{C_2H_4}}$
Step 6	$^*C_2H_5CO + {}^*H \overset{K_6}{} {}^*C_2H_5CHO + *$	$TOF_{C_2H_5CHO} = k_6 \theta_{*H} \theta_{*C_2H_5CO}$
Step 7	$^*C_2H_5 + {}^*H \overset{K_7}{} C_2H_6(g) + 2^*$	$TOF_{C_2H_6} = k_7 \theta_{*H} \theta_{*C_2H_5}$
Step 8	$^*C_2H_5CHO \overset{K_8}{} C_2H_5CHO(g) + *$	$\theta_{*C_2H_5CHO} = \frac{P_{C_2H_5CHO}}{K_8(1+(K_1 P_{H_2})^{1/2}+K_2 P_{CO}+K_3 P_{C_2H_4})}$

[a] Considering steps 6 and 7 as the rate-limiting steps for propionaldehyde and ethane formation.
[b] $*$ represents vacant site.
[c] K_1 is the equilibrium adsorption parameter, k_{+1} is the forward rate constant, k_{-1} is the backward rate constant.

propionaldehyde and ethane formation in Table 2, using any of the elementary steps 1–4 as the RDS would lead to similar rate equations for ethane and propionaldehyde formation since they are common to both products. The difference in dependency of rate on the partial pressures for propionaldehyde and ethane formation in the power law equation (listed in Table 3) indicates that propionaldehyde and ethane formation involve different RDS. Thus, elementary steps 1–4 can be eliminated as the RDS. Step 7 is the only other alternative RDS for ethane formation. The RDS for propionaldehyde formation then may be elementary steps 5, 6, or 8. Postulating steps 5, 6, or 8 as the RDS for propionaldehyde formation yields LHHW I[a], II[a], and III[a] kinetic models, respectively, in Table 3. Details of derivation

TABLE 3

Comparison of Different Kinetic Models on Mn–Rh/SiO_2

Kinetic model	Rate-determining step	Equations	Δ%
Power law	—	$TOF_{C_2H_5CHO} = 274 P_{CO}^{0.34} P_{H_2}^{0.54} P_{C_2H_4}^{0.97}$	7.13
	—	$TOF_{C_2H_6} = 742 P_{CO}^{-0.97} P_{H_2}^{1.0} P_{C_2H_4}^{1.5}$	8.05
LHHW I[a]	Step 5	$TOF_{C_2H_5CHO} = \frac{213{,}000 P_{CO} \sqrt{P_{H_2}} P_{C_2H_4}}{(1+185 P_{CO}+14.4\sqrt{P_{H_2}}+0.0041 P_{C_2H_4})^2}$	19.57
	Step 7	$TOF_{C_2H_6} = \frac{283{,}000 P_{H_2} P_{C_2H_4}}{(1+185 P_{CO}+14.4\sqrt{P_{H_2}}+0.0041 P_{C_2H_4})^2}$	15.54
LHHW II[a]	Step 6	$TOF_{C_2H_5CHO} = \frac{475{,}000 P_{CO} P_{H_2} P_{C_2H_4}}{(1+92.7 P_{CO}+8.9\sqrt{P_{H_2}}+0.000086 P_{C_2H_4})^2}$	10.39
	Step 7	$TOF_{C_2H_6} = \frac{97{,}000 P_{H_2} P_{C_2H_4}}{(1+92.7 P_{CO}+8.9\sqrt{P_{H_2}}+0.000086 P_{C_2H_4})^2}$	16.62
LHHW II[b]	Step 6	$TOF_{C_2H_5CHO} = \frac{493{,}000 P_{CO} P_{H_2} P_{C_2H_4}}{(1+95.4 P_{CO}+9.2\sqrt{P_{H_2}}+0.13 P_{C_2H_4}+9.9 P_{CO}\sqrt{P_{H_2}} P_{C_2H_4})^2}$	9.85
	Step 7	$TOF_{C_2H_6} = \frac{103{,}000 P_{CO} P_{H_2} P_{C_2H_4}}{(1+95.4 P_{CO}+9.2\sqrt{P_{H_2}}+0.13 P_{C_2H_4}+9.9 P_{CO}\sqrt{P_{H_2}} P_{C_2H_4})^2}$	16.72
LHHW III[a]	Step 8	$TOF_{C_2H_5CHO} = \frac{225{,}000 P_{CO} P_{H_2} P_{C_2H_4}}{(1+235 P_{CO}+12.6\sqrt{P_{H_2}}+0.000052 P_{C_2H_4})}$	19.09
	Step 7	$TOF_{C_2H_6} = \frac{253{,}000 P_{H_2} P_{C_2H_4}}{(1+235 P_{CO}+12.6\sqrt{P_{H_2}}+0.000052 P_{C_2H_4})^2}$	24.86

[a] Model derived with assumption of $1 = \theta_{*CO} + \theta_{*H} + \theta_{*C_2H_5} + \theta_{*v}$.
[b] Model derived with assumption of $1 = \theta_{*CO} + \theta_{*H} + \theta_{*C_2H_5} + \theta_{*C_2H_5CO} + \theta_{*v}$.

and equation fitting procedure to estimate the model parameters have been previously reported (29) and will be briefly described here. Assumption of steps 6 and 7 as the RDS led to consideration of the rest of the steps in quasi-equilibrium (37) which allows relating adsorbate coverage of reactants and acyl intermediate to the partial pressure of reactants. In order to minimize the number of parameters in the adsorption isotherm equations and the LHHW kinetics model, θ_{*CO}, θ_{*H}, and $\theta_{*C_2H_4}$ were assumed to be significantly greater than $\theta_{*C_2H_5}$, $\theta_{*C_2H_5CO}$, and $\theta_{*C_2H_5CHO}$. Thus, the sum of fractional coverage of major adsorbates may be expressed as

$$1 = \theta_{*CO} + \theta_{*H} + \theta_{*C_2H_4} + \theta_{*v}, \qquad [5]$$

where θ_{*v} is the coverage of vacant sites. The above total coverage equation produced the LHHW II^a model in Table 3 which best fits the kinetic data of Rh/SiO_2 in a previous study (29) and those of $Mn{-}Rh/SiO_2$ in the present study. Table 3 summarizes the parameters and average percent error for the LHHW kinetic models.

The isotherm equations for adsorbate coverages that are derived from assumption of quasi-equilibrium with total coverage in Eq. [5] for the LHHW II^a model are listed in Table 2. These equations express adsorbate coverages solely in terms of the reactant partial pressures. Since the parameters in the adsorption group of the isotherm equation in Table 2 are identical to those in LHHW II^a model in Table 3, the isotherm equations for $\theta_{*C_2H_5CO}$ and θ_{*CO} with the value of parameters in the LHHW model in Table 3 can be written as

$$\theta_{*C_2H_5CO} = \frac{11{,}350 P_{CO} P_{H_2}^{1/2} P_{C_2H_4}}{\left(1 + 92.7 P_{CO} + 8.9 P_{H_2}^{1/2} + 0.000086 P_{C_2H_4}\right)} \qquad [6]$$

and

$$\theta_{*CO} = \frac{92.7 P_{CO}}{\left(1 + 92.7 P_{CO} + 8.9 P_{H_2}^{1/2} + 0.000086 P_{C_2H_4}\right)}. \qquad [7]$$

Equations [6] and [7] are used to determine the goodness of fit to measured coverage of $^*C_2H_5CHO$ and $^*CO$ to obtain the value of the whole group of parameters in their numerator. Equations [6] and [7] are plotted in Figs. 9 and 10, respectively. Equation [7] fits θ_{*CO} versus P_{H_2} and $P_{C_2H_4}$ data well but gives a significantly higher slope than that of θ_{*CO} versus P_{CO} data in Fig. 10. It should be noted that the integral linear CO absorbance is equivalent to θ_{*CO}, providing that the extinction coefficient of adsorbed CO is invariant with its coverage. Since tilted CO was not active for CO insertion, it was not included in the CO coverage estimate. Equation [6] fails to fit all the $\theta_{*C_2H_5CO}$ data.

Since the value of the measured $\theta_{*C_2H_5CO}$ is between 0.1 and 0.3, further inclusion of $\theta_{*C_2H_5CO}$ in the coverage equation [5] resulted in the LHHW II^b model, which consists

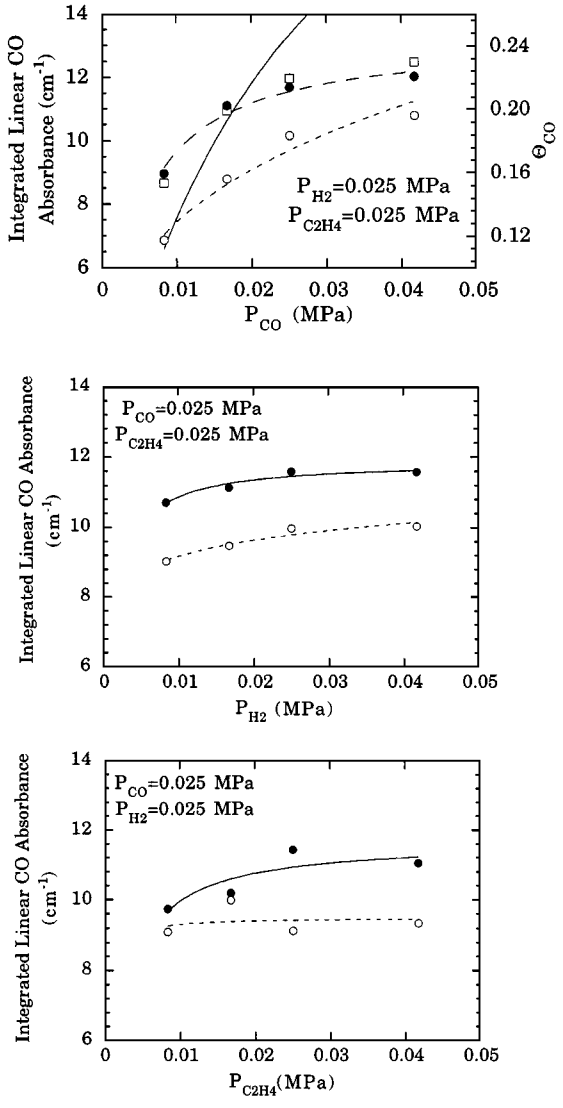

FIG. 10. Isotherms for CO adsorption integrated linear CO absorbance versus P_{CO}. Solid symbols represent Mn–Rh and open symbols represent Rh. Solid lines are plotted from Eq. [7]. Dashed lines (– – –) are plotted from CO isotherm equation from PSSA analysis.

of one more parameter than the LHHW II^a model. Although the additional parameter slightly improved the fit of rate data for C_2H_5CHO, the isotherm equations in the LHHW II^b model also fail to fit most of the measured coverage data of $^*CO$ and $^*C_2H_5CO$. Although the coverage of adsorbed C_2H_5CO measured by transient techniques was above 0.1, the adsorbed C_2H_5CO was not observed by IR. The inability of IR to detect adsorbed acyl species may be due to its low extinction coefficients.

Pseudo-Steady-State Approximation

Despite the good fit of LHHW II^a and LHHW II^b models for the rate data (i.e., TOF of propionaldehyde and ethane formation), their isotherm equations for coverage of

adsorbates do not explain the dependence of θ_{*CO} and $\theta_{*C_2H_5CO}$ on partial pressure of reactants. The goodness of the TOF fit may be explained by the number of available parameters in the LHHW kinetic model. For example, there are four adjustable parameters in the LHHW II^a model and five adjustable parameters in the LHHW II^b model for propionaldehyde formation. The inability of Eqs. [6] and [7] to accurately describe $\theta_{*C_2H_5CO}$ and θ_{*CO} data indicates that neither LHHW II^a nor LHHW II^b is the "true" kinetic mechanism.

Assumption of step 6, acyl hydrogenation, as the sole RDS may not be valid for propionaldehyde formation on Mn–Rh/SiO_2 catalysts. Assumption of step 6 as the RDS renders k_6 to be zero in the derivation of the $\theta_{*C_2H_5CO}$ isotherm equation in the LHHW II^a and the LHHW II^b models. Removing the assumption and applying the pseudo-steady-state approximation (36, 37) for the $\theta_{*C_2H_5CO}$ leads to

$$0 = r_{*C_2H_5CO} = k_5\theta_{*C_2H_5}\theta_{*CO} - k_{-5}\theta_{*C_2H_5CO}\theta_* - k_6\theta_{*C_2H_5CO}\theta_{*H}. \quad [8]$$

The reverse step of 6, k_{-6}, was not considered in Eq. [8] due to the low concentration of gaseous C_2H_5CHO (i.e., less than 0.8 mol% in the reactor effluent and the low concentration of $^*C_2H_5CHO$). Pseudo-steady-state approximation for $\theta_{*C_2H_5CO}$ intermediate is indeed consistent with experimental conditions when reactant flow and adsorbate concentration were maintained at steady-state conditions during measuring $\theta_{*C_2H_5CO}$. Solving Eq. [8] for $\theta_{*C_2H_5CO}$ gives

$$\theta_{*C_2H_5CO} = \frac{k_5\theta_{*C_2H_5}\theta_{*CO}}{k_{-5}\theta_* + k_6\theta_{*H}}. \quad [9]$$

Using the isotherm equations for $\theta_{*C_2H_5}$, θ_{*CO}, θ_{*H}, and θ_* from Table 2, $\theta_{*C_2H_5CO}$ can be rewritten as

$$\theta_{*C_2H_5CO} = \frac{k_5K_1^{1/2}K_2K_3K_4P_{H_2}^{1/2}P_{CO}P_{C_2H_4}}{(k_{-5} + k_6(K_1P_{H_2})^{1/2})(1 + K_2P_{CO} + (K_1P_{H_2})^{1/2} + K_3P_{C_2H_4})}. \quad [10]$$

Inclusion of the forward step 6 adds $k_6(K_1P_{H_2})^{1/2}$ into the denominator of Eq. [10]. The added term may account for decreasing $\theta_{*C_2H_5CO}$ with increasing P_{H_2}. Substituting θ_{*H} from Table 2 and $\theta_{*C_2H_5CO}$ from Eq. [10], the rate law $TOF_{C_2H_5CO} = k_6\theta_{*H}\theta_{*C_2H_5CO}$ is then expressed as

$$TOF_{C_2H_5CHO} = \frac{k_6K_1K_2K_3K_4k_5P_{H_2}P_{CO}P_{C_2H_4}}{(k_{-5} + k_6(K_1P_{H_2})^{1/2})(1 + K_2P_{CO} + (K_1P_{H_2})^{1/2} + K_3P_{C_2H_4})^2}. \quad [11]$$

The fit of TOF versus reactant partial pressure data to Eq. [11] yielded the values for the parameters. Equation [11] with the values of parameters is written as

$$TOF_{C_2H_5CHO} = \frac{51{,}000{,}000P_{H_2}P_{CO}P_{C_2H_4}}{(0.1 + 9.1 * 35.7P_{H_2}^{1/2})(1 + 1768P_{CO} + 35.7P_{H_2}^{1/2})^2} \quad [12]$$

with $\Delta\% = 10.39\%$, which is comparable to that of the LHHW II^a and the LHHW II^b models. Using the value of the parameters in Eq. [12], Eq. [10] can be rewritten as

$$\theta_{*C_2H_5CO} = \frac{6{,}014{,}000P_{H_2}^{1/2}P_{CO}P_{C_2H_4}}{(0.1 + 9.1 * 35.7P_{H_2}^{1/2})(1 + 1768P_{CO} + 35.7P_{H_2}^{1/2})} \quad [13]$$

for coverage of $\theta_{*C_2H_5CO}$. Figure 9 shows that the dashed lines which were plotted from Eq. [13] match well with the measured $\theta_{*C_2H_5CO}$ data. Also, k_6 in Eq. [13] has been independently determined to be 8.4 min^{-1} from pulse D_2 into H_2 transient response during $CO/H_2/C_2H_4$ reaction on the same catalyst. The surprising agreement for k_6 from modeling of rate data and experimental measurement of D_2 response provides support to the use of PSSA approach for kinetic analysis of Mn–Rh/SiO_2

Equation [13] further reveals that $k_{-5} = 0.1$ min^{-1} is significantly less than $k_6 = 9.1$ min^{-1}, indicating that step 5 is far from quasi-equilibrium and the forward step 6 is not the slowest step (i.e., RDS) for propionaldehyde formation on Mn–Rh/SiO_2. The RDS is the slowest step with the smallest rate constant among all the forward and backward steps in the reaction mechanism (37). Step 6 as the sole RDS suggests that the rate constants of all other steps including k_{-5} are much greater than k_6. This appears to be the case for reaction on Rh/SiO_2, but not on Mn–Rh/SiO_2. One major effect of Mn–Rh/SiO_2 that can be elucidated from comparison of k_{-5} and k_6 is that the significant decrease in k_{-5} brought about by Mn eradicates step 6 as the sole RDS, moving step 5 away from quasi-equilibrium, and blurring a single step as the RDS. Lack of a single step as the RDS caused the failure of the LHHW approach for the kinetic analysis of Mn–Rh/SiO_2 data. Blurring of the RDS for propionaldehyde formation was manifested in the difference in macroscopic rate data as well as residence time and coverage of adsorbed C_2H_5CO rather than coverage of adsorbed CO. Lack of variation in CO coverage on Rh/SiO_2 and Mn–Rh/SiO_2 can be explained by the quasi-equilibrium of CO adsorption which is evidenced by rapid exchange between adsorbed and gaseous CO during reaction on both catalysts as shown in Fig. 5. Blurring of the sole RDS by decreasing k_{-5} suggests that both step 5 (i.e., CO insertion) and step 6 (i.e., hydrogenation of $^*C_2H_5CO$) are kinetically significant steps in the formation of propionaldehyde on Mn–Rh/SiO_2.

CONCLUSIONS

The addition of MnO promoter to Rh/SiO_2 changes the dependence of the propionaldehyde formation rate, transient response, and adsorbed C_2H_5CO coverages on the reactant partial pressures. LHHW analysis shows that the assumption of a single RDS leads to a kinetic model which fits the rate data well, but its acyl isotherm equation cannot fit the observed coverage of adsorbed acyl intermediates. The response of ^{13}C propionaldehyde to ^{13}CO pulse reveals the uniform distribution of the active sites for propionaldehyde formation, and the absence of significant variation of wavenumber of adsorbed CO with partial pressure of reactants indicates the lack of interaction between adsorbed CO. Therefore, the failure of the LHHW kinetic model for description of the kinetics and coverage of adsorbates for the $CO/H_2/C_2H_4$ reaction on $Mn–Rh/SiO_2$ is not due to nonuniform active sites or adsorbate–adsorbate interaction. PSSA analysis reveals that both CO insertion and hydrogenation of adsorbed acyl intermediates are kinetically significant steps. Thus, the observed changes in rate law, transient response, and dependence of coverage and residence time of adsorbed acyl species on the reactant partial pressures can be attributed to modification of the RDS brought about by the Mn promoter.

This study shows that isotopic transient tracing coupled with *in situ* IR provides two levels of data for kinetic analysis: (i) LHHW and/or PSSA of rate data and (ii) analysis of isotherm equations for adsorbate coverage of CO and C_2H_5CO. Experimental and kinetic approaches employed in this study allow verification of kinetic models with mechanistic significance.

ACKNOWLEDGMENTS

The authors gratefully acknowledge the support of this research by the U.S. Department of Energy under Grant DG-FG-87PC79923 and partial support from the National Science Foundation under Grant CTS-942111996.

REFERENCES

1. Keim, W., *in* "Catalysis in C_1 Chemistry" (W. Keim, Ed.), p. 1. Reidel, Dordrecht, 1983.
2. Yoneda, Y., "Progress in C_1 Chemistry in Japan" (Research Association for C_1 Chemistry, Eds.). Elsevier, New York/Tokyo, 1989.
3. Arakawa, H., Hanaoka, T., Takeuchi, K., Matsuzaki, T., and Sugi, Y., *in* "Proceedings, 9th International Congress on Catalysis, Calgary, 1988" (M. J. Phillips and M. Ternan, Eds.), Vol. 2, p. 602. Chem. Institute of Canada, Ottawa, 1988.
4. Chuang, S. S. C., Tian, Y. H., Goodwin, J. G., Jr., and Wender, I., *J. Catal.* **96**, 449 (1985).
5. Chuang, S. S. C., Goodwin, J. G., Jr., and Wender, I., *J. Catal.* **92**, 416 (1985).
6. Kagami, S., Naito, S., and Tamaru, K., *J. Chem. Soc. Chem. Commun.*, 256 (1983).
7. Chuang, S. S. C., and Pien, S. I., *J. Catal.* **135**, 618 (1992).
8. Balakos, M. W., and Chuang, S. S. C., *Fuel Sci. Tech. Int.* **9**, 793 (1991).
9. Ichikawa, M., *ChemTech* **12**, 674 (1982).
10. Sachtler, W. M. H., and Ichikawa, M., *J. Phys. Chem.* **90**, 4752 (1986).
11. Hindermann, J. P., Hutchings, G. J., and Kiennemann, A., *Catal. Rev. Sci. Eng.* **53**, 1 (1993).
12. Ellgen, P. C., Bartley, W. J., Bhasin, M. M., and Wilson, T. P., *Adv. Chem. Ser.* **178**, 147 (1979).
13. Chuang, S. S. C., Brundage, M. A., and Balakos, M. W., *App. Catal. A: General* **151**, 333 (1997).
14. van den Berg, F. G. A., Glezer, J. H. E., and Sachtler, W. M. H., *J. Catal.* **93**, 340 (1985).
15. Fukushima, T., Arakawa, H., and Ichikawa, M., *J. Chem. Soc. Chem. Comm.* 729 (1985).
16. Stevenson, S. A., Lisitsyn, A., and Knozinger, H., *J. Phys. Chem.* **94**, 1576 (1990).
17. de Jong, K. P., Glezer, J. H. E., Kuipers, H. P. C. E., Knoester, A., and Emeis, C. A., *J. Catal.* **146**, 237 (1994).
18. Ichikawa, M., Hoffmann, P., and Fukuoka, A., *J. Chem. Soc. Chem. Commun.*, 1395 (1989).
19. Wilson, T. P., Kasai, P. H., and Ellgen, P. C., *J. Catal.* **69**, 193 (1981).
20. Sachtler, W. M. H., Shriver, D. F., Hollenberg, W. B., and Lang, A. F., *J. Catal.* **92**, 429 (1985).
21. Horwitz, C. P., and Shriver, D. F., *Adv. Organometallic Chem.* **23**, 219 (1984).
22. Chuang, S. S. C., Srinivas, G., and Brundage, M. A., *Energy Fuels* **10**, 524 (1996).
23. Jordan, D. S., and Bell, A. T., *J. Phys. Chem.* **90**, 4797 (1986).
24. Balakos, M. W., and Chuang, S. S. C., *J. Catal.* **151**, 253 (1995).
25. de Pontes, M., Yokomizo, G. H., and Bell, A. T., *J. Catal.* **104**, 147 (1987).
26. Shannon, S., and Goodwin, J., Jr., *Chem. Rev.* **95**, 677 (1995).
27. Chuang, S. S. C., Brundage, M. A., Balakos, M. W., and Srinivas, G., *Appl. Spectrosc.* **49**, 1151 (1995).
28. Sen, B., and Vannice, M. A., *J. Catal.* **113**, 52 (1988).
29. Balakos, M. W., and Chuang, S. S. C., *J. Catal.* **151**, 266 (1995).
30. Srinivas, G., and Chuang, S. S. C., *React. Kinet. Catal. Lett.* **48**, 613 (1992).
31. Chuang, S. S. C., and Pien, S. I., *J. Mol. Catal.* **55**, 12 (1989).
32. Weller, S. W., *Catal. Rev. Sci. Eng.* **34**, 227 (1992).
33. Boudart, M., "Kinetics of Heterogeneous Catalysis." Princeton Univ. Press, Princeton, NJ, 1984.
34. Boudart, M., *Ind. Eng. Chem. Fundam.* **25**, 656 (1986).
35. Mazaki, R., and Inoue, H., "Rate Equations of Solid-Catalyzed Reactions." Univ. of Tokyo Press, Tokyo, 1991.
36. Hill, C. G., Jr., "An Introduction to Chemical Engineering Kinetics and Reactor Design." Wiley, New York, 1977.
37. Tamaru, K., *in* "Catalysis: Science and Technology" (J. Anderson and M. Boudart, Eds.), Vol. 9, p. 87. Springer-Verlag, Berlin/Heidelberg/New York, 1991.